

## Perspectives on Antiferromagnetic Spintronics

Kang Wang\*, Vineetha Bheemarasetty, Junhang Duan, Shiyu Zhou, Gang Xiao\*

*Department of Physics, Brown University, Providence, Rhode Island 02912, USA*

### Abstract

Although the development of spintronic devices has advanced significantly over the past decade with the use of ferromagnetic materials, the extensive implementation of such devices has been limited by the notable drawbacks of these materials. Antiferromagnets claim to resolve many of these shortcomings leading to faster, smaller, more energy-efficient, and more robust electronics. Antiferromagnets exhibit many desirable properties including zero net magnetization, imperviousness to external magnetic fields, intrinsic high-frequency dynamics with a characteristic precession frequency on the order of terahertz (THz), and the ability to serve as passive exchange-bias materials in multiple magnetoresistance (MR)-based devices. In this Perspective article, we will discuss the fundamental physics of magnetic structures in antiferromagnets and their interactions with external stimuli such as spin current, voltage, and magnons. A discussion on the challenges lying ahead is also provided along with an outlook of future research directions of these systems.

---

\* Author to whom correspondence should be addressed. Electronic mail: [kang\\_wang@brown.edu](mailto:kang_wang@brown.edu) (K. Wang), [gang\\_xiao@brown.edu](mailto:gang_xiao@brown.edu) (G. Xiao).

## I. INTRODUCTION

In the context of spintronics, notable research efforts have focused on ferromagnetic materials while antiferromagnets [Fig. 1(a)] were regarded as “extremely interesting from a theoretical viewpoint” but futile in applications (see the Nobel lecture of Louis Néel who has discovered antiferromagnetism in the 1930s).<sup>1</sup> This stood true for about half a century until the employment of ferromagnetic/antiferromagnetic exchange bias in spin valves [Fig. 1(b)] which were commercialized in hard disk recording heads in the early 1990s (see reviews relating to the exchange bias<sup>2,3</sup>). More recently, several properties of antiferromagnets that make use of the exchange enhancement, spin-orbit interactions, and the interplay between spin torques and spin textures have been discovered [Figs. 1(c) and (d)]. These properties make antiferromagnetic materials outstanding candidates for next-generation spintronic applications, leading to a new paradigm of antiferromagnetic spintronics (see reviews relating to antiferromagnetic spintronics<sup>4-10</sup>).

Unlike ferromagnetic materials, antiferromagnets do not produce stray fields which can disturb neighboring circuits. This is highly favorable for reducing device size and compels device elements to be stable against external fields. Moreover, antiferromagnets exhibit intrinsic resonance frequencies in the terahertz (THz) range due to the exchange enhancement effect, thereby filling in the “Terahertz gap” between electronics and photonics.<sup>11</sup> This frequency range is much higher than that of ferromagnets whose frequencies lie in the gigahertz (GHz) range. The high-frequency spin dynamics show promise for high-speed antiferromagnetic spintronics with signal writing, processing, and detection in the THz regime (see related review articles<sup>9,12</sup>). Control over antiferromagnetic order has already been achieved by electrical switching, optical excitation, and heat-assisted magnetic recording [Fig. 1(c)]. The electrical writing of information in ferromagnets, such as electrical switching of magnetization, has been demonstrated by using spin-polarized current (see reviews relating to spin Hall effect and Rashba-Edelstein effect<sup>13-15</sup>). The electrical writing of antiferromagnets has also been verified in ways similar to their ferromagnetic counterparts (see reviews relating to electrical manipulations of antiferromagnetic

order<sup>5-7,16</sup>). The antiferromagnetic order can also be electrically detected by multiple methods including the magnetoresistance (MR) effect, inverse spin Hall effect, ferromagnetic resonance, second harmonic response of anomalous Hall effect (AHE) and anisotropic MR (AMR) [Fig. 1(c)] (see reviews relating to detection of the antiferromagnetic order<sup>6,7,17</sup>). Novel magnetic structures such as antiferromagnetic domain walls and skyrmions [Fig. 1(d)] have recently attracted significant attention (see reviews relating to magnetic skyrmions<sup>18-22</sup>). Antiferromagnetic domain walls and skyrmions can move with much higher velocities in comparison to their ferromagnetic counterparts. Moreover, antiferromagnetic skyrmions are not affected by the skyrmion Hall effect and exhibit a more temperature-activated diffusive motion. All these excellent properties of antiferromagnets make them increasingly relevant to future high-performance spintronics.

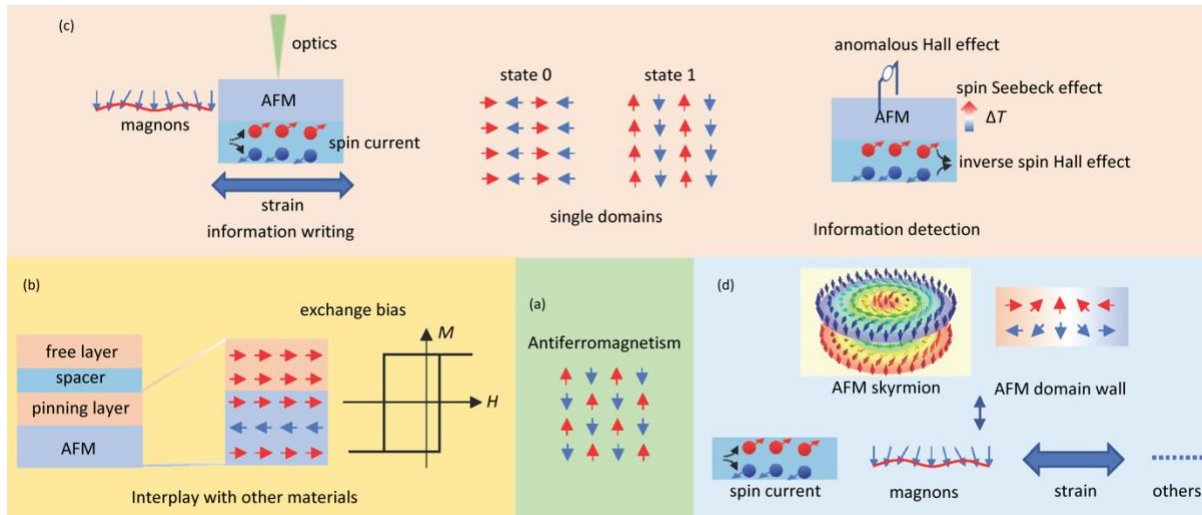


**FIG. 1.** (a) Schematic depiction of an antiferromagnetic order. (b) Interplay of antiferromagnets with other materials. Exchange bias is formed in antiferromagnetic/ferromagnetic interfacial systems and manifests as a field-shift in the hysteresis loop. Exchange bias plays a passive role in applications such as spin valves and magnetic tunnel junctions. (c) Writing and detection of single domains in antiferromagnets. (d) Antiferromagnetic domain walls and skyrmions that interact with external stimuli of spin current, magnons, or strain.

In this perspective, we present recent advances in the fundamental physics of magnetic structures in antiferromagnets and their interactions with external stimuli. Furthermore, we present a discuss on future research directions of these systems.

## II. MANIPULATIONS AND DETECTION OF ANTIFERROMAGNETIC ORDER

Due to its relative immunity to external fields and its inability to generate dipolar stray fields, antiferromagnetic memory is considered superior to its ferromagnetic counterpart in the storage and stability of magnetic states. However, these characteristics also make it difficult to manipulate and detect antiferromagnetic order, on which resides the antiferromagnetic memory.

Among multiple mechanisms, electrical control over antiferromagnetic order is of great importance to spintronic research. Several methods have been shown to successfully achieve magnetization switching including the spin Hall effect<sup>23-29</sup> and inverse spin-galvanic effect<sup>30-32</sup>. The in-plane spin accumulation at the interface between a spin Hall solid and an antiferromagnet exerts spin-orbit torques (SOTs) on the spins, which can lead to magnetization switching of either the collinear (such as NiO)<sup>23-26</sup> or non-collinear (such as Mn<sub>3</sub>Sn)<sup>27-29</sup> [Figs. 2(a) and (b)] antiferromagnetic order. Room-temperature electrical switching has also been realized in antiferromagnets such as CuMnAs<sup>30,32</sup> and Mn<sub>2</sub>Au<sup>31</sup> with no adjacent spin Hall materials [Figs. 2(d)-(h)]. The switching in these cases is attributed to the current-induced Néel SOT generated in antiferromagnets with specific structural and magnetic properties where the relativistic staggered internal field is strongly coupled to the antiferromagnetic order. Olejník et al. has demonstrated that THz-range switching can be achieved, paving the way for antiferromagnetic memory with ultrafast electrical writing speed.<sup>32</sup> In 2020, Nair et al. demonstrated electrical switching in the magnetically intercalated transition metal dichalcogenide Fe<sub>1/3</sub>NbS<sub>2</sub>.<sup>33</sup> In this system, the switching is driven by the antidamping-like component of the spin-transfer torque, which differs from the mechanism of the field-like torque induced switching in CuMnAs and Mn<sub>2</sub>Au.

The key to the development of the next-generation spintronic technology is the ability to effectively manipulate antiferromagnetic order. To improve the efficiency of electrical manipulation, one must either enhance the charge-to-spin conversion of the spin Hall materials adjacent to neighboring antiferromagnets or improve the SOT generation efficiency in those antiferromagnets without the

assistance of spin Hall materials. Large spin Hall effect has been observed in heavy metals with strong spin-orbit coupling such as Pt,<sup>34-36</sup>  $\beta$ -Ta,<sup>37,38</sup> and  $\beta$ -W.<sup>39,40</sup> The spin Hall effect is caused by either the intrinsic mechanism of a non-zero Berry curvature or the impurity-induced skew scattering or side jump. Alloying can be used to enhance the extrinsic scattering.<sup>41-51</sup> On the other hand, the Berry curvature-induced intrinsic spin Hall effect can be improved by investigating topological materials with spin-orbit coupling and spin-momentum locking in surface and/or bulk states [Fig. 2(c)]. In addition to topological insulators such as Bi<sub>2</sub>Se<sub>3</sub>,<sup>52</sup> Cr-doped (Bi<sub>0.5</sub>Sb<sub>0.5</sub>)<sub>2</sub>Te<sub>3</sub>,<sup>53</sup> Bi<sub>1.5</sub>Sb<sub>0.5</sub>Te<sub>1.7</sub>Se<sub>1.3</sub>,<sup>54</sup> and Weyl/Dirac semimetals WTe<sub>2</sub><sup>55-58</sup> that have been verified in experiments, other materials including Weyl/Dirac semimetals TaAs,<sup>59</sup> IrO<sub>2</sub>,<sup>60</sup> W<sub>3</sub>Ta,<sup>61</sup> PtTe<sub>2</sub>,<sup>62</sup> ZrSiTe,<sup>63</sup> LaAlSi and LaAlGe<sup>64</sup> have been theorized to be intriguing potential candidates. Experimental demonstrations can be achieved by multiple methods including magnetotransport measurements along with a macro-spin analysis,<sup>34,37-40,49</sup> harmonic measurements,<sup>48</sup> spin-torque ferromagnetic resonance (FMR),<sup>36,43,45,46,50,51</sup> spin pumping along with the inverse spin Hall effect,<sup>42,47</sup> and spin Hall magnetoresistance.<sup>44,65,66</sup> A large spin Hall effect enables the development of ultrafast and energy-efficient antiferromagnetic spintronics such as magnetic random-access memory (MRAM) and spin-logic devices.<sup>67,68</sup>

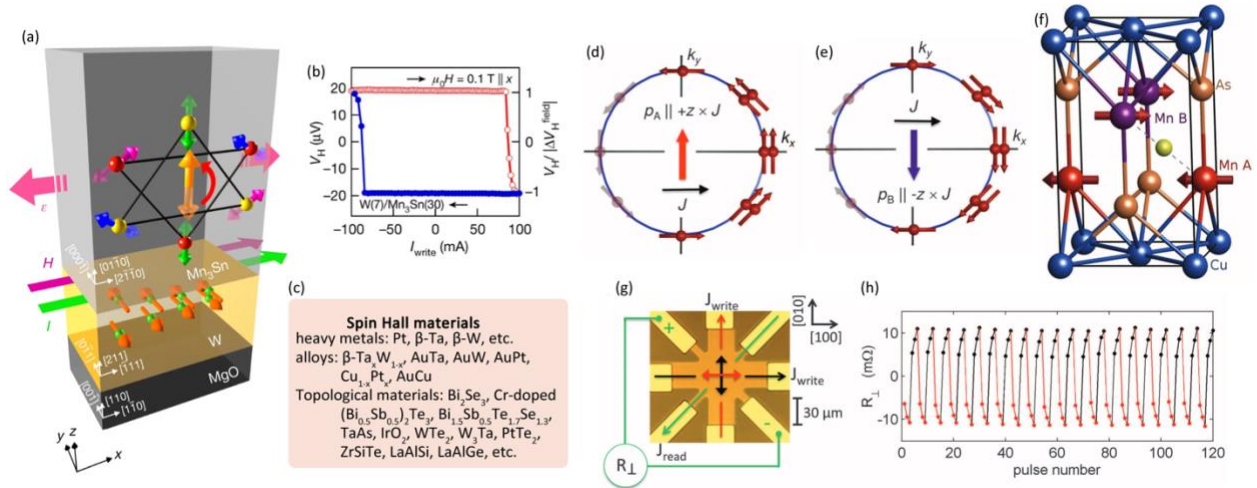


**FIG. 2.** (a) Schematic depiction of spin-orbit torque-driven switching of antiferromagnetic order in a noncollinear antiferromagnet Mn<sub>3</sub>Sn. An electric current (green arrow) flowing in the W layer generates a spin current (green

spheres) with spin polarizations perpendicular to the Kagome plane of  $\text{Mn}_3\text{Sn}$ . The spin current exerts spin torques on Mn moments in three antiferromagnetic sublattices, leading to the magnetization switching.<sup>29</sup> (b) Hall voltage  $V_H$  and volume fraction of the switching domain  $V_H/|\Delta V_H^{\text{field}}|$  as a function of the write current  $I_{\text{write}}$  flowing in the multilayer at room temperature. A bias field of 0.1 T along the  $x$  direction is applied.<sup>29</sup> Reproduced with permission from Higo et al., Nature 607, 474 (2022). Copyright 2022 Springer Nature. (c) A list of spin Hall materials. (d), (e) Schematic of the inverse spin galvanic effect in inversion asymmetric Rashba spin textures with opposite senses of the inversion asymmetry. A non-equilibrium redistribution of carriers in the in-plane momentum  $k_{x,y}$  space results in a net in-plane spin polarization.<sup>30</sup> (f)  $\text{CuMnAs}$  crystal structure and antiferromagnetic order. The two Mn sublattices A and B have opposite spins.<sup>30</sup> (g) Optical microscopy image of the device for current-driven switching in  $\text{CuMnAs}$ .<sup>30</sup> (h) Transverse resistance  $R_{\perp}$  variation after applying three successive writing pulses alternatively along the [100] and [010] directions to the device in (g). Current pulses have a pulse width of 50 ms and an amplitude of  $4 \times 10^6 \text{ A} \cdot \text{cm}^{-2}$ .<sup>30</sup> Reproduced with permission from Wadley et al., Science 351, 587 (2016). Copyright 2016 AAAS Publishing.

According to symmetry analysis, the charge-to-spin conversion is also expected in antiferromagnets such as  $\text{Mn}_3\text{Sn}$  [Figs. 3(a) and (b)],<sup>30,69</sup>  $\text{Mn}_3\text{GaN}$ ,<sup>70</sup> and  $\text{Mn}_2\text{Au}$ <sup>71,72</sup> where the spin polarization of spin current converted from a charge current is determined by symmetry conditions. All these materials are noncollinear antiferromagnets in which the pronounced charge-to-spin conversion efficiency is relevant to their topological band. We may infer more antiferromagnets with a large charge-spin interconversion efficiency from anomalous Hall investigations as the spin Hall and anomalous Hall effects share the same mechanisms.<sup>73</sup> One example is a magnetically intercalated transition metal dichalcogenide  $\text{Co}_{1/3}\text{NbS}_2$  [Fig. 3(c)].  $\text{Co}_{1/3}\text{NbS}_2$  was shown to exhibit a large anomalous Hall effect [Figs. 3(d)-(f)] with spins aligned in-plane collinearly along with a small out-of-plane ferromagnetic component (approximately  $0.0013 \mu_B$  per Co) below the ordering temperature  $T_N = 29 \text{ K}$ .<sup>74</sup> Tenasini et al. has shown that the anomalous Hall conductance of  $\text{Co}_{1/3}\text{NbS}_2$  is approximately  $0.6 e^2/h$  per layer when normalized to the number of contributing atomic planes [Fig. 3(e) and (f)], although it only has a very weak ferromagnetism.<sup>75</sup> This value approaches the value of a quantized anomalous Hall conductance suggest a topologically nontrivial band induced by the antiferromagnetic state.<sup>76</sup> Building on this, one may expect a large charge-to-spin conversion efficiency in  $\text{Co}_{1/3}\text{NbS}_2$ . Full quantization of the anomalous

Hall conductance together with a maximum charge-spin interconversion efficiency may be achieved by changing the carrier density through gating or doping to tune the Fermi level to a nontrivial band edge.

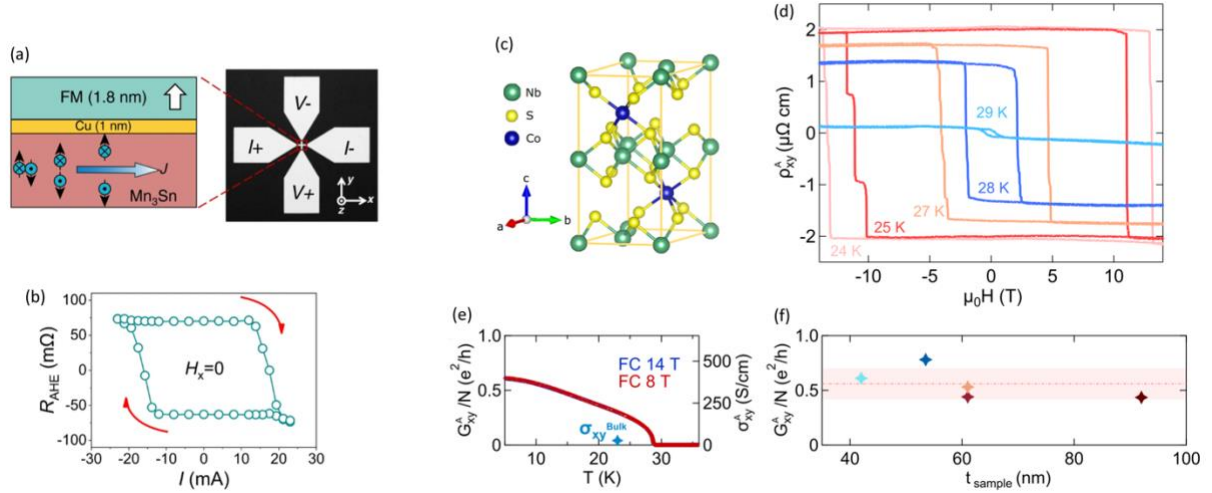


**FIG. 3.** (a) Schematic of  $\text{Mn}_3\text{Sn}(7 \text{ nm})/\text{Cu}(1 \text{ nm})/\text{ferromagnetic}(1.8 \text{ nm})$  stack along with optical microscopy image of the device used for electron transport measurements. A charge current flowing in the  $\text{Mn}_3\text{Sn}$  layer generates a spin current with spin polarizations along both  $y$  and  $z$  directions.<sup>69</sup> (b) Current-induced switching of magnetization characterized by the anomalous Hall resistance  $R_{\text{AHE}}$  in the absence of an external magnetic field.<sup>69</sup> Reproduced with permission from Hu et al., Nat. Commun. 13, 4447 (2022). Copyright 2022 Springer Nature. (c) Crystallographic unit cell of  $\text{Co}_{1/3}\text{NbS}_2$ .<sup>75</sup> (d) Anomalous Hall resistivity  $\rho_{xy}^A$  versus the perpendicular magnetic field  $\mu_0 H$  at different temperatures.<sup>75</sup> (e) Temperature dependence of the anomalous Hall conductivity  $\sigma_{xy}^A$  as well as the normalized anomalous Hall conductance per atomic layer  $G_{xy}^A/N$  for field cooling in 8 T and 14 T. The blue diamond represents the  $\sigma_{xy}^A$  in a bulk crystal.<sup>75</sup> (f)  $G_{xy}^A/N$  measured at 5 K for different samples with variable thickness.<sup>75</sup> Reproduced with permission from Tenasini et al., Phys. Rev. Research 2, 023051 (2020). Copyright 2020 American Physical Society.

The spin current, typically associated with charge flow, is unfavorable for ultralow power spintronic applications due to the non-negligible Joule heating effects that arise over time along with a short nanometer-scale propagation length.<sup>10</sup> A magnon current, which describes the precessing motion of spin moments, successfully addresses these shortcomings with a propagation length of several micrometers. Not only must we first understand the principles of this recently discovered form of spin current, but we must also study how the magnon current interacts with antiferromagnetic order. A

magnon-torque-induced full magnetization switching has been achieved in ferromagnetic NiFe<sup>77</sup> and SrRuO<sub>3</sub><sup>78</sup> as well as in ferrimagnetic Y<sub>3</sub>Fe<sub>5</sub>O<sub>12</sub> (YIG).<sup>79</sup> In these studies, the magnon current is induced by the spin current generated in spin Hall materials. The efficiency of magnon-torque-induced switching is determined by the magnon-related spin torque efficiency and interfacial spin transparency which may be further improved by fabricating epitaxial interfaces. The efficient manipulation of antiferromagnetic order is crucial for spintronic applications with low energy consumptions, however magnon-torque-induced manipulations of other antiferromagnets have yet to be demonstrated.

The antiferromagnetic order can be electrically detected by multiple methods such as the magnetoresistance (MR) effect, inverse spin Hall effect, ferromagnetic resonance, second harmonic response of anomalous Hall effect (AHE) and anisotropic MR (AMR).<sup>6,7,17</sup> Most of these technologies take advantage of additional layers as detectors [Fig. 1(d)]. On the other hand, the anomalous Hall detection of antiferromagnetic order has drawn much attention in recent years [Fig. 1(e)]. Large anomalous Hall effect has been identified in some noncollinear antiferromagnets such as Mn<sub>3</sub>Ge and Mn<sub>3</sub>Sn where a non-vanishing Berry curvature exists.<sup>80-83</sup> The anomalous Hall effect vanishes in collinear antiferromagnets. Band-structure engineering may help obtain a more pronounced anomalous Hall effect, as aforementioned discussions for Co<sub>1/3</sub>NbS<sub>2</sub>.

Antiferromagnets have been applied to a wide variety of applications. One example is the exchange bias in antiferromagnetic/ferromagnetic systems. Exchange bias manifests as a shift in the hysteresis loop and plays a passive role in applications. In single-domain studies, the in-plane exchange bias field facilitates zero-field perpendicular magnetization switching by eliminating the need for external longitudinal fields.<sup>84,85</sup> In addition, the exchange bias has also been utilized to pin the adjacent ferromagnetic layer in magnetic tunnel junctions (MTJs).<sup>86-95</sup> A MTJ typically consists of two ferromagnetic layers separated by an insulating layer where the tunneling magnetoresistance (TMR) is controlled by the relative magnetization orientation between the two ferromagnetic layers. The utilization of ferromagnetic free layers, however, limits miniaturization of devices in applications. Alternatively,

antiferromagnetic MTJs allow for smaller devices that are more stable against external fields.

Antiferromagnetic MTJs such as CuMnAs/GaP/CuMnAs have been theoretically proposed.<sup>96,97</sup> Although a sizable TMR effect is expected, perfect interfacial structures are needed, and disorder and interface roughness may weaken the TMR effect greatly. On the other hand, a different antiferromagnetic MTJ based on RuO<sub>2</sub>/TiO<sub>2</sub>/RuO<sub>2</sub> has been suggested [Fig. 4] where the TMR effect is largely independent of interfacial irregularities.<sup>98</sup> RuO<sub>2</sub> is a room-temperature metallic antiferromagnet with a rutile structure where Ru atoms at the center and corners of a unit cell have opposite spins.<sup>99</sup> RuO<sub>2</sub> has drawn much attention recently owing to its intriguing properties such as a crystal Hall effect,<sup>100</sup> a magnetic spin Hall effect,<sup>101,102</sup> and spin-splitting without spin-orbit coupling.<sup>103</sup> Shao et al. has reported a large TMR of approximately 500% in RuO<sub>2</sub>/TiO<sub>2</sub>/RuO<sub>2</sub> which they attribute to distinct spin-polarized conduction channels that are inherited from the antiferromagnetic order and are sustained in the presence of spin-orbit coupling.<sup>98</sup> The spin-polarized conduction channels are not unique to RuO<sub>2</sub> and exists in a wide range of materials that violate space-time  $\hat{P}\hat{T}$  symmetry [Fig. 4(a)]. A spin-neutral current passing through such an antiferromagnet generates a spin current with a momentum-dependent spin polarization and may switch the antiferromagnetic free layer [Figs. 4(a) and (b)]. The fabrication of such antiferromagnetic MTJs for experimental investigation, although unexplored, may be achieved by a chemical vapor deposition technique which has been shown to be useful in the epitaxial growth of CrO<sub>2</sub>/SnO<sub>2</sub> films on TiO<sub>2</sub> substrates.<sup>104</sup>

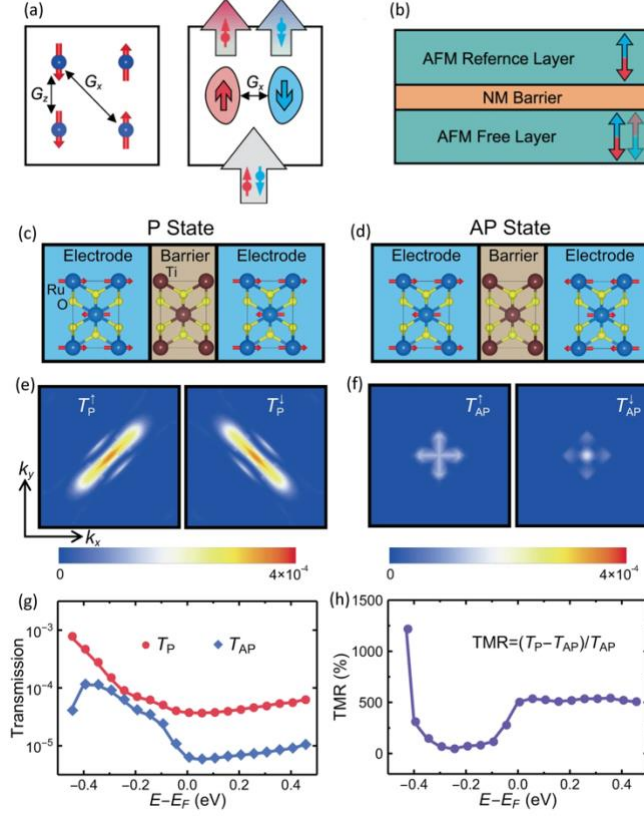


**FIG. 4.** (a) Schematics of the atomic structure (left) and non-spin-degenerate Fermi surface (right) in a compensated antiferromagnet where the space-time  $\hat{P}\hat{T}$  symmetry is violated. A spin-neutral current passing through this antiferromagnet remains globally spin neutral but has a momentum-dependent spin polarization.<sup>98</sup> (b) Schematic of an antiferromagnetic tunnel junction with a non-magnetic barrier.<sup>98</sup> (c), (d) The atomic and magnetic structures of  $\text{RuO}_2/\text{TiO}_2/\text{RuO}_2$  for (c) parallel and (d) antiparallel configuration.<sup>98</sup> (e), (f) The calculated  $k_{x,y}$ -resolved transmission in the Brillouin zone for the antiferromagnetic tunnel junction in (e) parallel and (f) antiparallel states.<sup>98</sup> (g) Total transmission as a function of energy in parallel and antiparallel states.<sup>98</sup> (h) Tunneling magnetoresistance as a function of energy.<sup>98</sup> Reproduced with permission from Shao et al., Nat. Commun. 12, 7061 (2021). Copyright 2021 Springer Nature.

### III. ANTIFERROMAGNETIC DOMAIN WALLS AND SKYRMIONS

In addition to manipulating and detecting single domains in antiferromagnets, novel magnetic structures have also been observed and are gaining notable attention. Antiferromagnetic domain walls and skyrmions have been observed in multiple systems including antiferromagnetic compounds and Ruderman-Kittel-Kasuya-Yoshida (RKKY)-coupled antiferromagnetic multilayers, as discussed below.

Magnetic domain walls and skyrmions are of great relevance to spintronic applications owing to their desirable properties including non-volatility, stability, and efficient controllability.

To date, most research efforts have demonstrated antiferromagnetic domain walls in collinear antiferromagnets such as  $\text{Co}_{1-x}\text{Tb}_x$ ,<sup>105</sup>  $\text{Gd}_x\text{Co}_{1-x}$ ,<sup>106</sup>  $\text{Tm}_3\text{Fe}_5\text{O}_{12}$ ,<sup>107</sup>  $\text{Cr}_2\text{O}_3$ ,<sup>108</sup> and Bismuth-substituted yttrium iron garnet ( $\text{BiYIG}$ )<sup>109</sup> [Fig. 5(a)]. Antiferromagnetic domain walls in noncollinear antiferromagnets have received much less attention. Difficulties involve writing as well as real-space and real-time imaging of antiferromagnetic domain walls. We expect to be able to write antiferromagnetic domain walls using electric current, magnons, strain, and optics, similarly to their ferromagnetic counterparts.<sup>9,12</sup> Imaging of antiferromagnetic domain walls may be achieved by space-resolved techniques including magneto-optic Kerr effect (MOKE) microscopy<sup>110</sup> and scanning thermal gradient microscopy (STGM).<sup>111</sup> Notably, STGM is a bulk-sensitive technique and is more suitable for probing domain walls in noncollinear antiferromagnets with a pronounced anomalous Nernst effect.<sup>111</sup> Along with the detection of domain walls, manipulations by spin currents<sup>112</sup> and spin waves<sup>113</sup> have yet to be demonstrated.

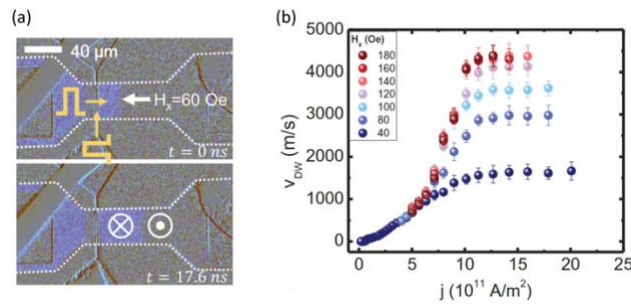


**FIG. 5.** (a) Magneto-optic Kerr effect (MOKE) microscope images of domain-wall motion in the collinear antiferromagnetic Bismuth-substituted yttrium iron garnet ( $\text{BiYIG}$ ), captured at  $t = 0$  ns and  $t = 17.6$  ns. A vertical current pulse is applied to create domain walls. A horizontal current pulse of  $1.65 \times 10^{12}$  A/m<sup>2</sup> is applied to drive domain-wall motion.<sup>109</sup> (b) Domain-wall velocity  $v_{\text{DW}}$  versus driving current density  $j$  at various in-plane magnetic field  $H_x$ .<sup>109</sup> Reproduced with permission from Caretta et al., Science 370, 1438 (2020). Copyright 2020 AAAS Publishing.

Antiferromagnetic domain walls can move very efficiently with velocities exceeding 1 km/s, which may even reach the relativistic limit [Fig. 5(b)].<sup>109,114</sup> This is a consequence of the characteristically low effective mass arising from the large internal exchange torques. In addition, the velocity is restricted by the magnon group velocity. This is contrary to their ferromagnetic counterparts where large damping leads to dynamic instabilities such as Walker breakdown and limits the mobility of ferromagnetic domain walls.<sup>115,116</sup> Although numerous studies have demonstrated the efficient motion of antiferromagnetic domain walls driven by spin currents,<sup>105,106,109,117,118</sup> investigations of additional controls of current-driven domain-wall motion is required. For example, Guan et al. has shown that domain-wall motion velocity may be finely tuned by the gate voltage through controlling the interfacial oxidation state.<sup>118</sup> On the other hand, theoretical research has demonstrated that spin waves can move domain walls in a more energy-efficient manner by momentum transfer.<sup>119-124</sup> This theory, however, has not yet been supported by experiments. The interplay between magnons and domain walls has already been studied in ferromagnetic systems. Wagner et al. demonstrated the channeling of spin waves inside nano-sized domain walls in a 40-nm-thick Ni<sub>81</sub>Fe<sub>19</sub> film.<sup>125</sup> In addition, Hämäläinen et al. has controlled spin-wave propagation across domain walls by modifying the domain-wall configuration.<sup>126</sup> While 90° head-to-head or tail-to-tail domain walls are transparent to spin waves, head-to-tail domain-wall configuration hinders spin-wave propagation. Moreover, theoretical works have predicted that domain walls can also be utilized to manipulate the phase of spin waves.<sup>127-132</sup> More recently, Han et al. has experimentally verified such a phase-shifting effect and has also shown a spin-wave-driven domain-wall motion in ferromagnetic Pt/[Co/Ni]<sub>9</sub>/Ru multilayers.<sup>133</sup> How exactly spin waves interact with antiferromagnetic domain walls remains unexplored, although this may be studied in ways similar to their ferromagnetic counterparts. Research on this topic may provide a new avenue to efficiently manipulating antiferromagnetic domain walls and to controlling spin waves up to the THz range which can benefit applications in non-volatile memory and magnonic logic devices.

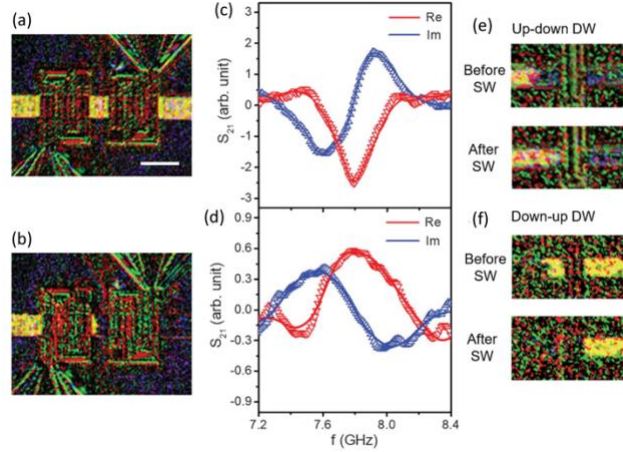


**FIG. 6.** (a), (b) Magneto-optic Kerr effect (MOKE) microscope images of a device composed of a ferromagnetic strip and two antennae for spin wave generation and detection. The magnetic films under study consist of substrate/Ti(8 nm)/Pt(7 nm)/[Co(0.4 nm)/Ni(0.35~0.4 nm)]<sub>9</sub>/Ru(3 nm). The bright and dark regions in the strip represent domains with up and down magnetization, respectively. The scale bar in (a) is 10 nm. In (a), the ferromagnetic state is a single-domain state, and in (b), a domain wall is located between two antennae.<sup>133</sup> (c), (d) Transmission spectra  $S_{21}$  for (a) and (b), respectively. A phase-shifting effect is observed when the spin wave propagates through a domain wall. A microwave power of  $0.4 \mu\text{W}$  was used for the measurement.<sup>133</sup> (e), (f) MOKE images of the motion of (e) up-down and (f) down-up domain walls driven by spin waves. A microwave power of  $2.2 \text{ mW}$  at the resonant frequency of  $8.8 \text{ GHz}$  was applied for the measurement.<sup>133</sup> Reproduced with permission from Han et al., Science 366, 1121 (2019). Copyright 2019 AAAS Publishing.

In addition to domain walls, skyrmions are topologically non-trivial magnetic structures and have also attracted significant attention. Ferromagnetic skyrmions have been observed in non-centrosymmetric bulk magnets as well as heterostructures with inversion symmetry broken where antisymmetric Dzyaloshinskii-Moriya interaction (DMI)<sup>134,135</sup> exists.<sup>19,20,136</sup> More recently, antiferromagnetic skyrmions have also been detected in RKKY-coupled antiferromagnetic multilayers such as Pt/Co/Co<sub>0.19</sub>Fe<sub>0.56</sub>B<sub>0.25</sub>/Ir/Co/CoFeB/W<sup>137</sup> and Co/Ru/Pt/Co<sup>138</sup> as well as magnetic exchange coupled Co/Gd/Pt,<sup>139</sup> Pt/CoGd [Fig. 7],<sup>140</sup> and GdFeCo<sup>141</sup> films. Skyrmions, however, were only observed in a nonzero, finite field range in these antiferromagnets. Zero-field stabilization of skyrmions is crucial in skyrmionic applications. Field-free creation and manipulation of ferromagnetic skyrmions have been verified by engineering interfacial exchange bias,<sup>142,143</sup> modifying the device geometry,<sup>144,145</sup> as well as by

using external stimuli such as strain engineering,<sup>146</sup> chemisorption and desorption.<sup>147</sup> Zero-field creation and manipulation of antiferromagnetic skyrmions remains elusive. Given that antiferromagnets are immune to the external field, it is thereby difficult to create zero-field antiferromagnetic skyrmions through exchange-bias engineering. Instead, a biasing interaction provided by an additional magnetic layer may help to create zero-field skyrmions.<sup>138</sup> Moreover, external stimuli such as the strain, optics, and magnons, may also help to create zero-field skyrmions. The key is to switch magnetization in a defined region forming a magnetic bubble which may then be transformed into a skyrmion stabilized by the antisymmetric DMI.

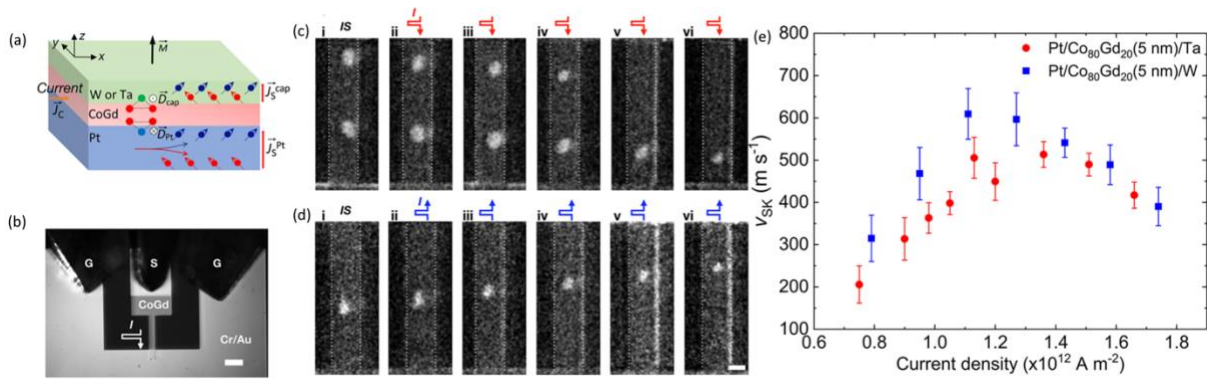


**FIG. 7.** (a) Schematic representation of the Pt/CoGd/W(or Ta) films where antiferromagnetic skyrmions in CoGd were studied. Both the bottom Pt and the capping W or Ta layers contribute to the interfacial Dzyaloshinskii-Moriya interaction (DMI) for skyrmion stabilization. In addition, both the bottom and capping layers can generate spin currents to drive skyrmion motion.<sup>140</sup> (b) Optical image of the device used for current-driven skyrmion motion. The scale bar is 30  $\mu\text{m}$ .<sup>140</sup> (c), (d) Sequence of magneto-optic Kerr effect (MOKE) microscope images presenting the current-driven skyrmion motion in Pt/CoGd/Ta. (c) Positive and (d) negative current pulses with a pulse width of 5 ns and amplitudes of (c)  $1.5 \times 10^{12} \text{ A/m}^2$  and (d)  $1.8 \times 10^{12} \text{ A/m}^2$  were applied to drive skyrmion motion. A perpendicular field of -10 mT was applied to stabilize the skyrmions. The scale bar is 5  $\mu\text{m}$ .<sup>140</sup> (e) The velocity of antiferromagnetic skyrmions in Pt/Co<sub>80</sub>Gd<sub>20</sub>(5 nm)/Ta and Pt/Co<sub>80</sub>Gd<sub>20</sub>(5 nm)/W as a function of current density.<sup>140</sup> Reproduced with permission from Quessab et al., Nano Lett. 22, 6091 (2022). Copyright 2022 American Chemical Society.

In contrast to ferromagnetic skyrmions which experience transverse motion known as the skyrmion Hall effect owing to the gyroscopic force, antiferromagnetic skyrmions<sup>137-140,148,149</sup> along with

skyrmioniums<sup>150</sup> experience a reduced or non-existent skyrmion Hall effect as skyrmions on the two sublattices experience opposite gyroscopic forces which cancel each other out. Moreover, antiferromagnetic skyrmions are marked by a higher mobility [Figs. 7(c)-(e)] and a reduced size enabled by a lower dipolar field. These desirable properties make these magnetic textures preferable for spintronic applications.

Magnetic domain walls and skyrmions can serve as effective agents for next-generation beyond-CMOS data storage,<sup>151-153</sup> logic,<sup>154-156</sup> probabilistic computing,<sup>157-160</sup> and neuromorphic computing<sup>161</sup> devices. For these applications, understanding the dynamics of domain walls and skyrmions is crucial. For example, Wang et al. has verified a true random number generator by using local dynamics of a single ferromagnetic skyrmion.<sup>160</sup> Moreover, the noise produced by domain walls and skyrmions is crucial in magnetic field sensing and determines the sensing capability of a sensor device.<sup>162-164</sup> Recently, Wang et al. has demonstrated a high-performance anomalous Hall sensor based on RKKY-coupled magnetic thin films [Fig. 8].<sup>163</sup> The RKKY-coupled film-based anomalous Hall sensors effectively address the trade-off between the sensor size, sensing capability, and stability, all of which are desirable for microscale sensing under a wide range of environmental conditions. Studying the noise signatures of magnetic structures is equally important to understanding their magnetization dynamics as well as to the development and implementation of these spintronic devices. Questions remain as to how these magnetic textures interact with each other as well as with local pinning centers, how the dynamics of these magnetic textures affect the electrical transport properties, and what roles the interactions and topology play in the dynamics. To answer these questions, one may need to modulate the pinning conditions of these magnetic systems either by introducing inherent random defects through varying growth conditions or by implementing artificial pinning centers through advanced thin film fabrication, lithography, irradiation, ion implantation, and laser ablation methods. Moreover, it may be necessary to monitor the real-time responses of these magnetic textures to external stimuli along with simultaneous measurements of electric

transport properties which may be achieved by an electronic noise measurement system integrated with magnetic imaging techniques such as a MOKE microscope.

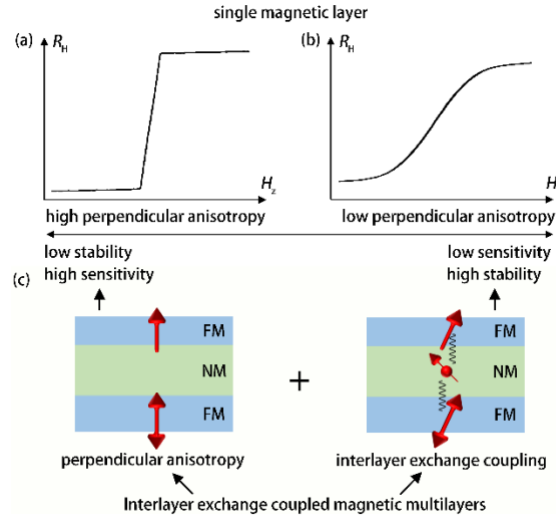


**FIG. 8.** (a), (b) Sketches of anomalous Hall loops of a single magnetic layer-based anomalous Hall sensor with (a) a high perpendicular magnetic anisotropy and (b) a low perpendicular anisotropy. The sensitivity increases with increasing the perpendicular anisotropy, but the stability is consequently reduced. This points to a trade-off between the sensing capability and stability for single magnetic layer-based anomalous Hall sensors. (c) In Ruderman-Kittel-Kasuya-Yoshida (RKKY)-coupled film-based anomalous Hall sensors, the RKKY interaction enhances the stability in addition to the perpendicular anisotropy that can be tuned to yield high sensitivity.<sup>163</sup> Reproduced with permission from Wang et al., Phys. Rev. Appl. 13, 064009 (2020). Copyright 2020 American Physical Society.

Recently, a theoretical work has predicted the existence of an interlayer DMI in a RKKY-coupled magnetic film with an in-plane asymmetry in addition to the well-studied interfacial DMI.<sup>165</sup> The interlayer DMI governs a chiral magnetization across magnetic multilayers, which has been observed in some prototype systems [Fig. 9(a)].<sup>166-170</sup> The interlayer DMI originates either from crystalline asymmetry<sup>165</sup> or from the in-plane asymmetry of the interlayer exchange interaction (IEI) [Fig. 9(a)].<sup>167,169,170</sup> The interlayer and the intralayer DMIs provide two effective parameters to design and construct three-dimensional magnetic structures and devices. For this, it is essential to fabricate multilayers with an interlayer DMI that has a large effect on magnetization. One expects that the effects of the interlayer DMI may be improved by enhancing the interlayer DMI relative to the total energy,

either by increasing the interlayer DMI strength or by reducing the magnetic anisotropy and the strength of the symmetric IEI between the magnetic layers.<sup>169</sup> Fabricating multilayers with a large antisymmetric/symmetric exchange interaction ratio (*e.g.*, Rh/Fe/Ir) can improve the contribution from the crystalline asymmetry. This can be achieved by depositing magnetic multilayers with a spacer layer featured by a large spin-orbit coupling. On the other hand, the in-plane asymmetry of the IEI can be improved by fabricating wedge-shaped samples. Beyond a simple structure of two ferromagnetic layers separated by a spacer, one can also fabricate multilayers with a periodic structure to study the magnetic structures in these multilayers. Fernández-Pacheco et al.<sup>166</sup> and Han et al.<sup>167</sup> have shown an asymmetric response of the interlayer DMI-governed chiral magnetization to the external magnetic field [Fig. 9(b)]. Moreover, Wang et al.<sup>169</sup> and Masuda et al.<sup>170</sup> have observed an asymmetric current-driven switching of the chiral magnetization which they attribute to the spin torque from the interlayer DMI [Figs. 9(c)-(e)]. In addition to single domains, the interactions of magnetic structures with external fields and spin currents are not well-understood and require further investigation. As suggested from the asymmetric current-driven switching,<sup>169</sup> one expects that, if there is a magnetic domain wall, the wall will also show an asymmetric response to spin currents. The velocity of the domain wall motion will be asymmetric with respect to the spin current with different polarities. Note that the motion of domain walls governed by the interfacial DMI is only asymmetric with respect to the external magnetic field.<sup>171,172</sup> If demonstrated, the spin-current-driven asymmetric motion of the domain wall will provide more selectivity and controllability for designing domain wall-based racetrack memory and spin logic devices. In addition, one also anticipates that antiferromagnetic skyrmions in such multilayers with interlayer DMI will exhibit an unconventional response to the external field and spin transfer torques.

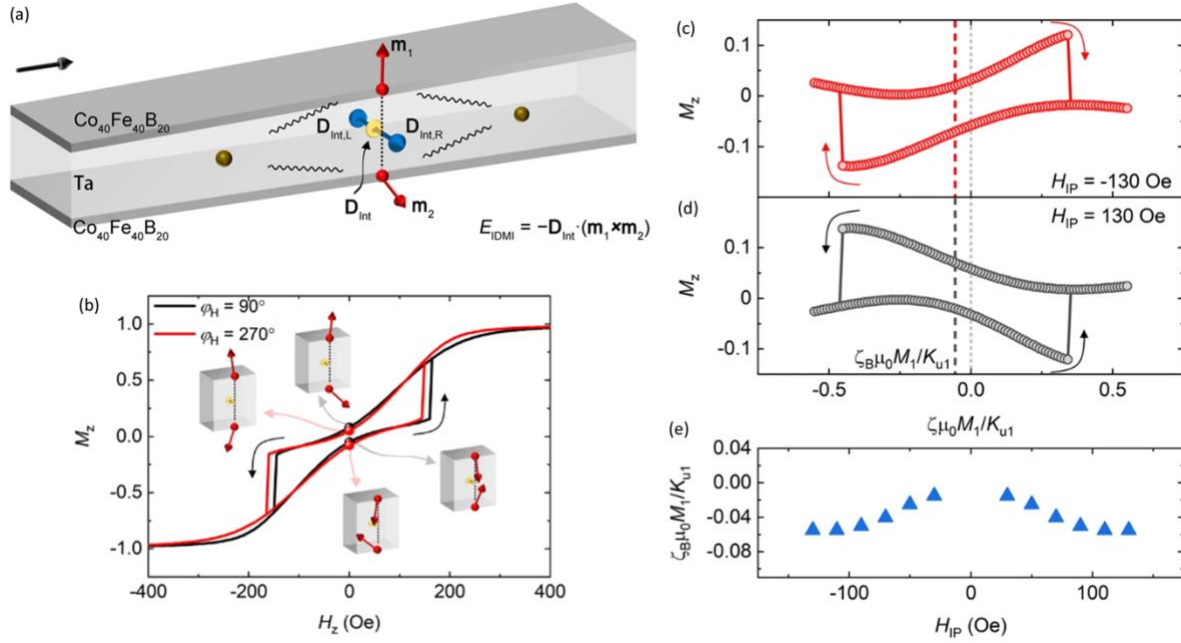


**FIG. 9.** (a) Schematic of the interlayer Dzyaloshinskii-Moriya interaction (DMI) in a multilayer of MgO/Co<sub>40</sub>Fe<sub>40</sub>B<sub>20</sub>/Ta/Co<sub>40</sub>Fe<sub>40</sub>B<sub>20</sub>/MgO where an in-plane asymmetry of the interlayer exchange coupling (IEC) between two magnetic layers (black arrow along which the spacer-layer and ferromagnetic layer thicknesses increase) exists.<sup>173</sup> The interlayer DMI mediated by the left part ( $\mathbf{D}_{\text{Int,L}}$ , blue arrow) and the right part ( $\mathbf{D}_{\text{Int,R}}$ , blue arrow) cannot be compensated with each other. This leads to a nonzero net interlayer DMI vector ( $\mathbf{D}_{\text{Int}}$ , yellow arrow) which governs a chiral magnetization across multilayers to lower the interlayer DMI energy  $E_{\text{Int}} = -\mathbf{D}_{\text{Int}} \cdot (\mathbf{m}_1 \times \mathbf{m}_2)$ . Wavy lines represent exchange interactions between spins in the ferromagnetic layers mediated by conduction electrons in the spacer layer.<sup>169</sup> (b) Numerical calculations of asymmetric hysteresis loops for  $M_z$  when applying an in-plane magnetic field  $H_{\text{IP}} = 100$  Oe along  $\varphi_H = 90^\circ$  (black curve, parallel to the black arrow in (a)) as well as  $\varphi_H = 270^\circ$  (red curve, antiparallel to the black arrow in (a)).<sup>169</sup> (c), (d) Numerical calculations of the asymmetric spin-orbit torque (SOT)-driven switching with the application of a (c) negative (antiparallel to the black arrow in (a)) and (d) positive (parallel to the black arrow in (a))  $H_{\text{IP}}$ . The current is applied along the black arrow direction in (a). A bias SOT is observed when an interlayer DMI exists.<sup>169</sup> (e) The bias SOT as a function of the  $H_{\text{IP}}$ .<sup>169</sup> Reproduced with permission from Wang et al., Commun. Phys. 4, 10 (2021). Copyright 2021 Springer Nature.

#### IV. CONCLUSIONS

In this article, we provide a brief review of recent advances in the manipulation and detection of single domains in antiferromagnets. The keys to next-generation spintronic technology include electrical control and detection of spins in antiferromagnets along with ways to increase the efficiency of spin

manipulation. We present a perspective on some new materials such as  $\text{Co}_{1/3}\text{NbS}_2$  which have been shown to possess a giant anomalous Hall effect. The underlying physics and charge-spin interconversion efficiency in such systems, however, is not yet clear. We also discuss applications of antiferromagnets in spintronic devices such as antiferromagnetic MTJs with a large TMR which demand further investigation in experiments.

In addition, we review recent studies on domain walls and skyrmions in antiferromagnets which address their higher mobility in comparison to their ferromagnetic counterparts. Moreover, antiferromagnetic skyrmions overcome the skyrmion Hall effect and exhibit a more temperature-activated diffusive motion. We also discuss the interactions of domain walls and skyrmions with spin waves or magnons by addressing questions such as how to use spin waves to manipulate these spin textures, and in turn how these magnetic structures affect the amplitudes and phases of the spin waves. Given that magnetic multilayers with both the interfacial and interlayer DMIs provide new platforms to construct 3D magnetic structures, we also address how to incorporate a pronounced interlayer DMI into a synthetic antiferromagnet. These magnetic structures may show nontrivial responses to external stimuli which will undoubtedly expand the scope of spintronic applications.

## ACKNOWLEDGEMENTS

G.X. acknowledges funding support from the National Science Foundation (NSF) under Grant No. OMA-1936221 and Grant No. DMR-2202514.

## REFERENCES

- <sup>1</sup> L. Néel, *Science* **174**, 985 (1971).
- <sup>2</sup> J. Nogués and I. K. Schuller, *J. Magn. Magn. Mater.* **192**, 203 (1999).
- <sup>3</sup> W. Zhang and K. M. Krishnan, *Mater. Sci. Eng.: R: Rep.* **105**, 1 (2016).
- <sup>4</sup> E. Gomonay and V. Loktev, *Low Temp. Phys.* **40**, 17 (2014).

- 5 J. Sklenar, W. Zhang, M. B. Jungfleisch, W. Jiang, H. Saglam, J. E. Pearson, J. B. Ketterson, and  
A. Hoffmann, *AIP Adv.* **6**, 055603 (2016).
- 6 T. Jungwirth, X. Marti, P. Wadley, and J. Wunderlich, *Nat. Nanotechnol.* **11**, 231 (2016).
- 7 I. Fina and X. Marti, *IEEE Trans. Magn.* **53**, 2500107 (2016).
- 8 Y. Wang, C. Song, J. Zhang, and F. Pan, *Prog. Nat. Sci.: Mater. Int.* **27**, 208 (2017).
- 9 V. Baltz, A. Manchon, M. Tsoi, T. Moriyama, T. Ono, and Y. Tserkovnyak, *Rev. Mod. Phys.* **90**,  
015005 (2018).
- 10 D. Xiong, Y. Jiang, K. Shi, A. Du, Y. Yao, Z. Guo, D. Zhu, K. Cao, S. Peng, and W. Cai,  
*Fundam. Res.* **2**, 522 (2022).
- 11 S. Dhillon, M. Vitiello, E. Linfield, A. Davies, M. C. Hoffmann, J. Booske, C. Paoloni, M.  
Gensch, P. Weightman, and G. Williams, *J. Phys. D: Appl. Phys.* **50**, 043001 (2017).
- 12 A. Kirilyuk, A. V. Kimel, and T. Rasing, *Rev. Mod. Phys.* **82**, 2731 (2010).
- 13 J. Sinova, S. O. Valenzuela, J. Wunderlich, C. Back, and T. Jungwirth, *Rev. Mod. Phys.* **87**, 1213  
(2015).
- 14 A. Manchon, H. C. Koo, J. Nitta, S. Frolov, and R. Duine, *Nat. Mater.* **14**, 871 (2015).
- 15 Q. Shao, P. Li, L. Liu, H. Yang, S. Fukami, A. Razavi, H. Wu, K. Wang, F. Freimuth, and Y.  
Mokrousov, *IEEE Trans. Magn.* **57**, 1 (2021).
- 16 H. Yan, Z. Feng, P. Qin, X. Zhou, H. Guo, X. Wang, H. Chen, X. Zhang, H. Wu, and C. Jiang,  
*Adv. Mater.* **32**, 1905603 (2020).
- 17 L. Šmejkal, A. H. MacDonald, J. Sinova, S. Nakatsuji, and T. Jungwirth, *Nat. Rev. Mater.* **7**, 482  
(2022).
- 18 X. Zhang, Y. Zhou, K. M. Song, T.-E. Park, J. Xia, M. Ezawa, X. Liu, W. Zhao, G. Zhao, and S.  
Woo, *J. Phys.: Condens. Matter* **32**, 143001 (2020).
- 19 C. Back, V. Cros, H. Ebert, K. Everschor-Sitte, A. Fert, M. Garst, T. Ma, S. Mankovsky, T.  
Monchesky, and M. Mostovoy, *J. Phys. D: Appl. Phys.* **53**, 363001 (2020).
- 20 Y. Tokura and N. Kanazawa, *Chem. Rev.* **121**, 2857 (2020).
- 21 S. Li, W. Kang, X. Zhang, T. Nie, Y. Zhou, K. L. Wang, and W. Zhao, *Mater. Horiz.* **8**, 854  
(2021).
- 22 K. Wang, V. Bheemarasetty, J. Duan, S. Zhou, and G. Xiao, *J. Magn. Magn. Mater.*, 169905  
(2022).
- 23 X. Chen, R. Zarzuela, J. Zhang, C. Song, X. Zhou, G. Shi, F. Li, H. Zhou, W. Jiang, and F. Pan,  
*Phys. Rev. Lett.* **120**, 207204 (2018).
- 24 T. Moriyama, K. Oda, T. Ohkochi, M. Kimata, and T. Ono, *Sci. Rep.* **8**, 14167 (2018).

- 25 I. Gray, T. Moriyama, N. Sivadas, G. M. Stiehl, J. T. Heron, R. Need, B. J. Kirby, D. H. Low, K.  
C. Nowack, and D. G. Schlom, *Phys. Rev. X* **9**, 041016 (2019).
- 26 L. Baldrati, O. Gomonay, A. Ross, M. Filianina, R. Lebrun, R. Ramos, C. Leveille, F. Fuhrmann,  
T. Forrest, and F. Maccherozzi, *Phys. Rev. Lett.* **123**, 177201 (2019).
- 27 Y. Takeuchi, Y. Yamane, J.-Y. Yoon, R. Itoh, B. Jinnai, S. Kanai, J. i. Ieda, S. Fukami, and H.  
Ohno, *Nat. Mater.* **20**, 1364 (2021).
- 28 G. Q. Yan, S. Li, H. Lu, M. Huang, Y. Xiao, L. Wernert, J. A. Brock, E. E. Fullerton, H. Chen,  
and H. Wang, *Adv. Mater.* **34**, 2200327 (2022).
- 29 T. Higo, K. Kondou, T. Nomoto, M. Shiga, S. Sakamoto, X. Chen, D. Nishio-Hamane, R. Arita,  
Y. Otani, and S. Miwa, *Nature* **607**, 474 (2022).
- 30 P. Wadley, B. Howells, J. Železný, C. Andrews, V. Hills, R. P. Campion, V. Novák, K. Olejník,  
F. Maccherozzi, and S. Dhesi, *Science* **351**, 587 (2016).
- 31 S. Y. Bodnar, L. Šmejkal, I. Turek, T. Jungwirth, O. Gomonay, J. Sinova, A. Sapozhnik, H.-J.  
Elmers, M. Kläui, and M. Jourdan, *Nat. Commun.* **9**, 348 (2018).
- 32 K. Olejník, T. Seifert, Z. Kašpar, V. Novák, P. Wadley, R. P. Campion, M. Baumgartner, P.  
Gambardella, P. Němec, and J. Wunderlich, *Sci. Adv.* **4**, eaar3566 (2018).
- 33 N. L. Nair, E. Maniv, C. John, S. Doyle, J. Orenstein, and J. G. Analytis, *Nat. Mater.* **19**, 153  
(2020).
- 34 L. Liu, O. Lee, T. Gudmundsen, D. Ralph, and R. Buhrman, *Phys. Rev. Lett.* **109**, 096602 (2012).
- 35 M.-H. Nguyen, D. Ralph, and R. Buhrman, *Phys. Rev. Lett.* **116**, 126601 (2016).
- 36 W. Zhang, W. Han, X. Jiang, S.-H. Yang, and S. SP Parkin, *Nat. Phys.* **11**, 496 (2015).
- 37 L. Liu, C.-F. Pai, Y. Li, H. Tseng, D. Ralph, and R. Buhrman, *Science* **336**, 555 (2012).
- 38 Q. Hao and G. Xiao, *Phys. Rev. B* **91**, 224413 (2015).
- 39 C.-F. Pai, L. Liu, Y. Li, H. Tseng, D. Ralph, and R. Buhrman, *Appl. Phys. Lett.* **101**, 122404  
(2012).
- 40 Q. Hao and G. Xiao, *Phys. Rev. Appl.* **3**, 034009 (2015).
- 41 B. Gu, I. Sugai, T. Ziman, G. Guo, N. Nagaosa, T. Seki, K. Takanashi, and S. Maekawa, *Phys.*  
*Rev. Lett.* **105**, 216401 (2010).
- 42 P. Laczkowski, J.-C. Rojas-Sánchez, W. Savero-Torres, H. Jaffrès, N. Reyren, C. Deranlot, L.  
Notin, C. Beigné, A. Marty, and J.-P. Attané, *Appl. Phys. Lett.* **104**, 142403 (2014).
- 43 M. Obstbaum, M. Decker, A. Greitner, M. Haertinger, T. Meier, M. Kronseder, K. Chadova, S.  
Wimmer, D. Ködderitzsch, and H. Ebert, *Phys. Rev. Lett.* **117**, 167204 (2016).
- 44 L. Zou, S. Wang, Y. Zhang, J. Sun, J. Cai, and S. Kang, *Phys. Rev. B* **93**, 014422 (2016).

45 P. Laczkowski, Y. Fu, H. Yang, J.-C. Rojas-Sánchez, P. Noel, V. Pham, G. Zahnd, C. Deranlot,  
S. Collin, and C. Bouard, *Phys. Rev. B* **96**, 140405 (2017).

46 R. Ramaswamy, Y. Wang, M. Elyasi, M. Motapothula, T. Venkatesan, X. Qiu, and H. Yang,  
*Phys. Rev. Appl.* **8**, 024034 (2017).

47 D. Qu, S. Huang, G. Guo, and C. Chien, *Phys. Rev. B* **97**, 024402 (2018).

48 L. Zhu, D. C. Ralph, and R. A. Buhrman, *Phys. Rev. Appl.* **10**, 031001 (2018).

49 L. Qian, K. Wang, Y. Zheng, and G. Xiao, *Phys. Rev. B* **102**, 094438 (2020).

50 N. Behera, H. Fulara, L. Bainsla, A. Kumar, M. Zahedinejad, A. Houshang, and J. Åkerman,  
*Phys. Rev. Appl.* **18**, 024017 (2022).

51 P. Wang, A. Migliorini, S. H. Yang, J. C. Jeon, I. Kostanovskiy, H. Meyerheim, H. Han, H.  
Deniz, and S. S. Parkin, *Adv. Mater.* **34**, 2109406 (2022).

52 Y. Wang, P. Deorani, K. Banerjee, N. Koirala, M. Brahlek, S. Oh, and H. Yang, *Phys. Rev. Lett.*  
**114**, 257202 (2015).

53 Y. Fan, P. Upadhyaya, X. Kou, M. Lang, S. Takei, Z. Wang, J. Tang, L. He, L.-T. Chang, and M.  
Montazeri, *Nat. Mater.* **13**, 699 (2014).

54 Y. Shiomi, K. Nomura, Y. Kajiwara, K. Eto, M. Novak, K. Segawa, Y. Ando, and E. Saitoh,  
*Phys. Rev. Lett.* **113**, 196601 (2014).

55 S. Shi, S. Liang, Z. Zhu, K. Cai, S. D. Pollard, Y. Wang, J. Wang, Q. Wang, P. He, and J. Yu,  
*Nat. Nanotechnol.* **14**, 945 (2019).

56 P. Song, C.-H. Hsu, G. Vignale, M. Zhao, J. Liu, Y. Deng, W. Fu, Y. Liu, Y. Zhang, and H. Lin,  
*Nat. Mater.* **19**, 292 (2020).

57 B. Zhao, D. Khokhriakov, Y. Zhang, H. Fu, B. Karpiak, A. M. Hoque, X. Xu, Y. Jiang, B. Yan,  
and S. P. Dash, *Phys. Rev. Research* **2**, 013286 (2020).

58 I. Kao, R. Muzzio, H. Zhang, M. Zhu, J. Gobbo, S. Yuan, D. Weber, R. Rao, J. Li, and J. H.  
Edgar, *Nat. Mater.* **21**, 1029 (2022).

59 Y. Sun, Y. Zhang, C. Felser, and B. Yan, *Phys. Rev. Lett.* **117**, 146403 (2016).

60 Y. Sun, Y. Zhang, C.-X. Liu, C. Felser, and B. Yan, *Phys. Rev. B* **95**, 235104 (2017).

61 E. Derunova, Y. Sun, C. Felser, S. Parkin, B. Yan, and M. Ali, *Sci. Adv.* **5**, eaav8575 (2019).

62 H. Xu, J. Wei, H. Zhou, J. Feng, T. Xu, H. Du, C. He, Y. Huang, J. Zhang, and Y. Liu, *Adv.*  
*Mater.* **32**, 2000513 (2020).

63 Y. Yen and G.-Y. Guo, *Phys. Rev. B* **101**, 064430 (2020).

64 T. Ng, Y. Luo, J. Yuan, Y. Wu, H. Yang, and L. Shen, *Phys. Rev. B* **104**, 014412 (2021).

65 Y.-T. Chen, S. Takahashi, H. Nakayama, M. Althammer, S. T. Goennenwein, E. Saitoh, and G.  
E. Bauer, *Phys. Rev. B* **87**, 144411 (2013).

66 J. Kim, P. Sheng, S. Takahashi, S. Mitani, and M. Hayashi, *Phys. Rev. Lett.* **116**, 097201 (2016).  
67 B. Behin-Aein, D. Datta, S. Salahuddin, and S. Datta, *Nat. Nanotechnol.* **5**, 266 (2010).  
68 L. Qian, W. Chen, K. Wang, X. Wu, and G. Xiao, *AIP Adv.* **8**, 115323 (2018).  
69 S. Hu, D.-F. Shao, H. Yang, C. Pan, Z. Fu, M. Tang, Y. Yang, W. Fan, S. Zhou, and E. Y.  
Tsymbal, *Nat. Commun.* **13**, 4447 (2022).  
70 T. Nan, C. X. Quintela, J. Irwin, G. Gurung, D.-F. Shao, J. Gibbons, N. Campbell, K. Song, S.-Y.  
Choi, and L. Guo, *Nat. Commun.* **11**, 4671 (2020).  
71 B. B. Singh and S. Bedanta, *Phys. Rev. Appl.* **13**, 044020 (2020).  
72 X. Chen, S. Shi, G. Shi, X. Fan, C. Song, X. Zhou, H. Bai, L. Liao, Y. Zhou, and H. Zhang, *Nat.*  
*Mater.* **20**, 800 (2021).  
73 N. Nagaosa, J. Sinova, S. Onoda, A. H. MacDonald, and N. P. Ong, *Rev. Mod. Phys.* **82**, 1539  
(2010).  
74 N. J. Ghimire, A. Botana, J. Jiang, J. Zhang, Y.-S. Chen, and J. Mitchell, *Nat. Commun.* **9**, 3280  
(2018).  
75 G. Terasini, E. Martino, N. Ubrig, N. J. Ghimire, H. Berger, O. Zaharko, F. Wu, J. Mitchell, I.  
Martin, and L. Forró, *Phys. Rev. Research* **2**, 023051 (2020).  
76 H. Tanaka, S. Okazaki, K. Kuroda, R. Noguchi, Y. Arai, S. Minami, S. Ideta, K. Tanaka, D. Lu,  
and M. Hashimoto, *Phys. Rev. B* **105**, L121102 (2022).  
77 Y. Wang, D. Zhu, Y. Yang, K. Lee, R. Mishra, G. Go, S.-H. Oh, D.-H. Kim, K. Cai, and E. Liu,  
*Science* **366**, 1125 (2019).  
78 D. Zheng, J. Lan, B. Fang, Y. Li, C. Liu, J. O. Ledesma-Martin, Y. Wen, P. Li, C. Zhang, and Y.  
Ma, *Adv. Mater.* **34**, 2203038 (2022).  
79 C. Guo, C. Wan, M. Zhao, C. Fang, T. Ma, X. Wang, Z. Yan, W. He, Y. Xing, and J. Feng, *Phys.*  
*Rev. B* **104**, 094412 (2021).  
80 H. Chen, Q. Niu, and A. H. MacDonald, *Phys. Rev. Lett.* **112**, 017205 (2014).  
81 S. Nakatsuji, N. Kiyohara, and T. Higo, *Nature* **527**, 212 (2015).  
82 N. Kiyohara, T. Tomita, and S. Nakatsuji, *Phys. Rev. Appl.* **5**, 064009 (2016).  
83 A. K. Nayak, J. E. Fischer, Y. Sun, B. Yan, J. Karel, A. C. Komarek, C. Shekhar, N. Kumar, W.  
Schnelle, and J. Kübler, *Sci. Adv.* **2**, e1501870 (2016).  
84 Y.-W. Oh, S.-h. Chris Baek, Y. Kim, H. Y. Lee, K.-D. Lee, C.-G. Yang, E.-S. Park, K.-S. Lee,  
K.-W. Kim, and G. Go, *Nat. Nanotechnol.* **11**, 878 (2016).  
85 A. van den Brink, G. Vermaas, A. Solignac, J. Koo, J. T. Kohlhepp, H. J. Swagten, and B.  
Koopmans, *Nat. Commun.* **7**, 10854 (2016).  
86 W. Butler, X.-G. Zhang, T. Schulthess, and J. MacLaren, *Phys. Rev. B* **63**, 054416 (2001).

- 87 J. Mathon and A. Umerski, *Phys. Rev. B* **63**, 220403 (2001).
- 88 M. Bowen, V. Cros, F. Petroff, A. Fert, C. Martinez Boubeta, J. L. Costa-Krämer, J. V. Anguita,  
A. Cebollada, F. Briones, and J. De Teresa, *Appl. Phys. Lett.* **79**, 1655 (2001).
- 89 S. Yuasa, T. Nagahama, A. Fukushima, Y. Suzuki, and K. Ando, *Nat. Mater.* **3**, 868 (2004).
- 90 S. S. Parkin, C. Kaiser, A. Panchula, P. M. Rice, B. Hughes, M. Samant, and S.-H. Yang, *Nat.*  
*Mater.* **3**, 862 (2004).
- 91 G. He, Y. Zhang, Y. Hu, X. Zhang, and G. Xiao, *Sens. Actuator A: Phys.* **331**, 112966 (2021).
- 92 G. He, Y. Zhang, and G. Xiao, *Phys. Rev. Appl.* **14**, 034051 (2020).
- 93 Y. Zhang, G. He, X. Zhang, and G. Xiao, *Appl. Phys. Lett.* **115**, 022402 (2019).
- 94 W. Zhang, Q. Hao, and G. Xiao, *Phys. Rev. B* **84**, 094446 (2011).
- 95 W. Zhang, G. Xiao, and M. J. Carter, *Phys. Rev. B* **83**, 144416 (2011).
- 96 P. Merodio, A. Kalitsov, H. Béa, V. Baltz, and M. Chshiev, *Appl. Phys. Lett.* **105**, 122403  
(2014).
- 97 M. Stamenova, R. Mohebbi, J. Seyed-Yazdi, I. Rungger, and S. Sanvito, *Phys. Rev. B* **95**, 060403  
(2017).
- 98 D.-F. Shao, S.-H. Zhang, M. Li, C.-B. Eom, and E. Y. Tsymbal, *Nat. Commun.* **12**, 7061 (2021).
- 99 T. Berlijn, P. C. Snijders, O. Delaire, H.-D. Zhou, T. A. Maier, H.-B. Cao, S.-X. Chi, M.  
Matsuda, Y. Wang, and M. R. Koehler, *Phys. Rev. Lett.* **118**, 077201 (2017).
- 100 L. Šmejkal, R. González-Hernández, T. Jungwirth, and J. Sinova, *Sci. Adv.* **6**, eaaz8809 (2020).
- 101 R. González-Hernández, L. Šmejkal, K. Výborný, Y. Yahagi, J. Sinova, T. Jungwirth, and J.  
Železný, *Phys. Rev. Lett.* **126**, 127701 (2021).
- 102 A. Bose, N. J. Schreiber, R. Jain, D.-F. Shao, H. P. Nair, J. Sun, X. S. Zhang, D. A. Muller, E. Y.  
Tsymbal, and D. G. Schlom, arXiv preprint arXiv:2108.09150 (2021).
- 103 K.-H. Ahn, A. Hariki, K.-W. Lee, and J. Kuneš, *Phys. Rev. B* **99**, 184432 (2019).
- 104 G.-X. Miao, G. Xiao, and A. Gupta, *EPL (Europhysics Letters)* **87**, 47006 (2009).
- 105 S. A. Siddiqui, J. Han, J. T. Finley, C. A. Ross, and L. Liu, *Phys. Rev. Lett.* **121**, 057701 (2018).
- 106 L. Caretta, M. Mann, F. Büttner, K. Ueda, B. Pfau, C. M. Günther, P. Helsing, A. Churikova, C.  
Klose, and M. Schneider, *Nat. Nanotechnol.* **13**, 1154 (2018).
- 107 S. Vélez, J. Schaab, M. S. Wörnle, M. Müller, E. Gradauskaite, P. Welter, C. Gutgsell, C. Nistor,  
C. L. Degen, and M. Trassin, *Nat. Commun.* **10**, 4750 (2019).
- 108 N. Hedrich, K. Wagner, O. V. Pylypovskiy, B. J. Shields, T. Kosub, D. D. Sheka, D. Makarov,  
and P. Maletinsky, *Nat. Phys.* **17**, 574 (2021).
- 109 L. Caretta, S.-H. Oh, T. Fakhru, D.-K. Lee, B. H. Lee, S. K. Kim, C. A. Ross, K.-J. Lee, and G.  
S. Beach, *Science* **370**, 1438 (2020).

- 110 T. Higo, H. Man, D. B. Gopman, L. Wu, T. Koretsune, O. M. van't Erve, Y. P. Kabanov, D.  
Rees, Y. Li, and M.-T. Suzuki, *Nat. Photonics* **12**, 73 (2018).
- 111 H. Reichlova, T. Janda, J. Godinho, A. Markou, D. Kriegner, R. Schlitz, J. Zelezny, Z. Soban, M.  
Bejarano, and H. Schultheiss, *Nat. Commun.* **10**, 5459 (2019).
- 112 J. Železný, Y. Zhang, C. Felser, and B. Yan, *Phys. Rev. Lett.* **119**, 187204 (2017).
- 113 D. R. Rodrigues, A. Salimath, K. Everschor-Sitte, and K. Hals, *Phys. Rev. Lett.* **127**, 157203  
(2021).
- 114 T. Shiino, S.-H. Oh, P. M. Haney, S.-W. Lee, G. Go, B.-G. Park, and K.-J. Lee, *Phys. Rev. Lett.*  
**117**, 087203 (2016).
- 115 N. L. Schryer and L. R. Walker, *J. Appl. Phys.* **45**, 5406 (1974).
- 116 G. S. Beach, C. Nistor, C. Knutson, M. Tsoi, and J. L. Erskine, *Nat. Mater.* **4**, 741 (2005).
- 117 S.-H. Yang, K.-S. Ryu, and S. Parkin, *Nat. Nanotechnol.* **10**, 221 (2015).
- 118 Y. Guan, X. Zhou, F. Li, T. Ma, S.-H. Yang, and S. S. Parkin, *Nat. Commun.* **12**, 5002 (2021).
- 119 E. G. Tveten, A. Qaiumzadeh, and A. Brataas, *Phys. Rev. Lett.* **112**, 147204 (2014).
- 120 S. K. Kim, Y. Tserkovnyak, and O. Tchernyshyov, *Phys. Rev. B* **90**, 104406 (2014).
- 121 W. Wang, M. Albert, M. Beg, M.-A. Bisotti, D. Chernyshenko, D. Cortés-Ortuño, I. Hawke, and  
H. Fangohr, *Phys. Rev. Lett.* **114**, 087203 (2015).
- 122 W. Yu, J. Lan, and J. Xiao, *Phys. Rev. B* **98**, 144422 (2018).
- 123 S.-H. Oh, S. K. Kim, J. Xiao, and K.-J. Lee, *Phys. Rev. B* **100**, 174403 (2019).
- 124 K.-W. Kim, S.-W. Lee, J.-H. Moon, G. Go, A. Manchon, H.-W. Lee, K. Everschor-Sitte, and K.-  
J. Lee, *Phys. Rev. Lett.* **122**, 147202 (2019).
- 125 K. Wagner, A. Kákay, K. Schultheiss, A. Henschke, T. Sebastian, and H. Schultheiss, *Nat.*  
*Nanotechnol.* **11**, 432 (2016).
- 126 S. J. Hämäläinen, M. Madami, H. Qin, G. Gubbiotti, and S. van Dijken, *Nat. Commun.* **9**, 4853  
(2018).
- 127 R. Hertel, W. Wulfhekel, and J. Kirschner, *Phys. Rev. Lett.* **93**, 257202 (2004).
- 128 C. Bayer, H. Schultheiss, B. Hillebrands, and R. L. Stamps, *IEEE Trans. Magn.* **41**, 3094 (2005).
- 129 S. Macke and D. Goll, in *Transmission and reflection of spin waves in the presence of Néel walls*,  
2010 (IOP Publishing), p. 042015.
- 130 J.-S. Kim, M. Stärk, M. Kläui, J. Yoon, C.-Y. You, L. Lopez-Diaz, and E. Martinez, *Phys. Rev. B*  
**85**, 174428 (2012).
- 131 F. Buijnsters, Y. Ferreiros, A. Fasolino, and M. Katsnelson, *Phys. Rev. Lett.* **116**, 147204 (2016).
- 132 J. Lan, W. Yu, and J. Xiao, *Nat. Commun.* **8**, 178 (2017).
- 133 J. Han, P. Zhang, J. T. Hou, S. A. Siddiqui, and L. Liu, *Science* **366**, 1121 (2019).

- 134 I. Dzyaloshinsky, *J. Phys. Chem. Solids* **4**, 241 (1958).
- 135 T. Moriya, *Phys. Rev.* **120**, 91 (1960).
- 136 K. Wang, L. Qian, W. Chen, S.-C. Ying, G. Xiao, and X. Wu, *Phys. Rev. B* **99**, 184410 (2019).
- 137 T. Dohi, S. DuttaGupta, S. Fukami, and H. Ohno, *Nat. Commun.* **10**, 5153 (2019).
- 138 W. Legrand, D. Maccariello, F. Ajejas, S. Collin, A. Vecchiola, K. Bouzehouane, N. Reyren, V. Cros, and A. Fert, *Nat. Mater.* **19**, 34 (2020).
- 139 X. Wang, A. R. Stuart, M. S. Swyt, C. M. Q. Flores, A. T. Clark, A. Fiagbenu, R. V. Chopdekar, P. N. Lapa, Z. Xiao, and D. Keavney, *Phys. Rev. Mater.* **6**, 084412 (2022).
- 140 Y. Quessab, J.-W. Xu, E. Cogulu, S. Finizio, J. r. Raabe, and A. D. Kent, *Nano Lett.* **22**, 6091 (2022).
- 141 Z. Li, J. Su, S.-Z. Lin, D. Liu, Y. Gao, S. Wang, H. Wei, T. Zhao, Y. Zhang, and J. Cai, *Nat. Commun.* **12**, 5604 (2021).
- 142 K. G. Rana, A. Finco, F. Fabre, S. Chouaieb, A. Haykal, L. Buda-Prejbeanu, O. Fruchart, S. Le Denmat, P. David, and M. Belmeguenai, *Phys. Rev. Appl.* **13**, 044079 (2020).
- 143 Y. Guang, I. Bykova, Y. Liu, G. Yu, E. Goering, M. Weigand, J. Gräfe, S. K. Kim, J. Zhang, and H. Zhang, *Nat. Commun.* **11**, 949 (2020).
- 144 F. Büttner, I. Lemesh, M. Schneider, B. Pfau, C. M. Günther, P. Hessian, J. Geilhufe, L. Caretta, D. Engel, and B. Krüger, *Nat. Nanotechnol.* **12**, 1040 (2017).
- 145 S. Finizio, K. Zeissler, S. Wintz, S. Mayr, T. Weßels, A. J. Huxtable, G. Burnell, C. H. Marrows, and J. Raabe, *Nano Lett.* **19**, 7246 (2019).
- 146 C. Feng, F. Meng, Y. Wang, J. Jiang, N. Mehmood, Y. Cao, X. Lv, F. Yang, L. Wang, and Y. Zhao, *Adv. Funct. Mater.* **31**, 2008715 (2021).
- 147 G. Chen, C. Ophus, A. Quintana, H. Kwon, C. Won, H. Ding, Y. Wu, A. K. Schmid, and K. Liu, *Nat. Commun.* **13**, 1350 (2022).
- 148 X. Zhang, Y. Zhou, and M. Ezawa, *Nat. Commun.* **7**, 10293 (2016).
- 149 J. Barker and O. A. Tretiakov, *Phys. Rev. Lett.* **116**, 147203 (2016).
- 150 J. Tang, Y. Wu, W. Wang, L. Kong, B. Lv, W. Wei, J. Zang, M. Tian, and H. Du, *Nat. Nanotechnol.* **16**, 1086 (2021).
- 151 K. Wang, L. Qian, S.-C. Ying, G. Xiao, and X. Wu, *Nanoscale* **11**, 6952 (2019).
- 152 S. S. Parkin, M. Hayashi, and L. Thomas, *Science* **320**, 190 (2008).
- 153 A. Fert, V. Cros, and J. Sampaio, *Nat. Nanotechnol.* **8**, 152 (2013).
- 154 Z. Luo, A. Hrabec, T. P. Dao, G. Sala, S. Finizio, J. Feng, S. Mayr, J. Raabe, P. Gambardella, and L. J. Heyderman, *Nature* **579**, 214 (2020).

- 155 Z. Yan, Y. Liu, Y. Guang, K. Yue, J. Feng, R. Lake, G. Yu, and X. Han, *Phys. Rev. Appl.* **15**,  
064004 (2021).
- 156 X. Zhang, M. Ezawa, and Y. Zhou, *Sci. Rep.* **5**, 9400 (2015).
- 157 J. Zázvorka, F. Jakobs, D. Heinze, N. Keil, S. Kromin, S. Jaiswal, K. Litzius, G. Jakob, P. Virnau,  
and D. Pinna, *Nat. Nanotechnol.* **14**, 658 (2019).
- 158 R. Ishikawa, M. Goto, H. Nomura, and Y. Suzuki, *Appl. Phys. Lett.* **119**, 072402 (2021).
- 159 Y. Jibiki, M. Goto, E. Tamura, J. Cho, S. Miki, R. Ishikawa, H. Nomura, T. Srivastava, W. Lim,  
and S. Auffret, *Appl. Phys. Lett.* **117**, 082402 (2020).
- 160 K. Wang, Y. Zhang, V. Bheemarasetty, S. Zhou, S.-C. Ying, and G. Xiao, *Nat. Commun.* **13**, 722  
(2022).
- 161 K. M. Song, J.-S. Jeong, B. Pan, X. Zhang, J. Xia, S. Cha, T.-E. Park, K. Kim, S. Finizio, and J.  
Raabe, *Nat. Electron.* **3**, 148 (2020).
- 162 Y. Zhang, K. Wang, and G. Xiao, *Appl. Phys. Lett.* **116**, 212404 (2020).
- 163 K. Wang, Y. Zhang, and G. Xiao, *Phys. Rev. Appl.* **13**, 064009 (2020).
- 164 K. Wang, Y. Zhang, S. Zhou, and G. Xiao, *Nanomaterials* **11**, 854 (2021).
- 165 E. Y. Vedmedenko, P. Riego, J. A. Arregi, and A. Berger, *Phys. Rev. Lett.* **122**, 257202 (2019).
- 166 A. Fernández-Pacheco, E. Vedmedenko, F. Ummelen, R. Mansell, D. Petit, and R. P. Cowburn,  
*Nat. Mater.* **18**, 679 (2019).
- 167 D.-S. Han, K. Lee, J.-P. Hanke, Y. Mokrousov, K.-W. Kim, W. Yoo, Y. L. Van Hees, T.-W.  
Kim, R. Lavrijsen, and C.-Y. You, *Nat. Mater.* **18**, 703 (2019).
- 168 S. D. Pollard, J. A. Garlow, K.-W. Kim, S. Cheng, K. Cai, Y. Zhu, and H. Yang, *Phys. Rev. Lett.*  
**125**, 227203 (2020).
- 169 K. Wang, L. Qian, S.-C. Ying, and G. Xiao, *Commun. Phys.* **4**, 10 (2021).
- 170 H. Masuda, T. Seki, Y. Yamane, R. Modak, K.-i. Uchida, J. i. Ieda, Y.-C. Lau, S. Fukami, and K.  
Takanashi, *Phys. Rev. Appl.* **17**, 054036 (2022).
- 171 K.-S. Ryu, L. Thomas, S.-H. Yang, and S. Parkin, *Nat. Nanotechnol.* **8**, 527 (2013).
- 172 K.-S. Ryu, S.-H. Yang, L. Thomas, and S. S. Parkin, *Nat. Commun.* **5**, 3910 (2014).
- 173 K. Wang, L. Qian, S.-C. Ying, and G. Xiao, *Phys. Rev. B* **102**, 144430 (2020).